PHYSICAL REVIEW B **88**, 161405(R) (2013)

Role of MgO barriers for spin and charge transport in Co/MgO/graphene nonlocal spin-valve devices

F. Volmer, M. Drögeler, E. Maynicke, N. von den Driesch, M. L. Boschen, G. Güntherodt, and B. Beschoten*
2nd Institute of Physics and JARA-FIT, RWTH Aachen University, D-52074 Aachen, Germany
(Received 28 May 2013; published 21 October 2013)

We investigate spin and charge transport in both single and bilayer graphene nonlocal spin-valve devices. An inverse dependence of the spin lifetime τ_s on the carrier mobility μ is observed in devices with large contact-resistance-area products ($R_cA > 1$ kΩ μm^2). Furthermore, we observe an increase of τ_s with increasing R_cA values, demonstrating that spin transport is limited by spin dephasing underneath the electrodes. In charge transport, we measure a second contact-induced Dirac peak at negative gate voltages in devices with larger R_cA values, demonstrating different transport properties in contact-covered and bare graphene parts. We argue that the existence of the second Dirac peak complicates the analysis of the carrier mobilities and the spin scattering mechanisms.

DOI: 10.1103/PhysRevB.88.161405 PACS number(s): 72.80.Vp, 72.25.−b, 72.25.Rb, 73.40.Cg

Graphene has drawn strong attention because of a measured spin-diffusion length of several microns at room temperature. While most spin-transport devices only exhibit spin lifetimes up to several hundred picoseconds at room temperature,[1–9] there are only a few reports with spin lifetimes above 1 ns.[10–12] Nevertheless, all experimental values of the spin lifetimes are several orders of magnitude shorter than theoretically predicted,[13,14] indicating that in present devices spin transport is limited by extrinsic sources of spin scattering. These include spin-orbit coupling by adatoms, edge effects, and ripples.[6,10,13,15–18] Additionally, spin scattering may result from the underlying substrate or the spin injection and detection contacts.[14,19,20] The importance of the latter might be indicated by recent electron spin resonance (ESR) experiments on graphene nanoribbons and small flakes that were only weakly coupled to the substrate and had no electrodes.[21,22] Interestingly, the measured spin lifetimes of localized spin states are at least 200 ns, while the estimated spin lifetimes of conduction electrons are 30 ns, which is larger than any reported value from electrical Hanle spin precession measurements.

In this Rapid Communication, we investigate the influence of MgO barriers on spin- and charge-transport properties by fabricating both single-layer (SLG) and bilayer graphene (BLG) nonlocal spin-valve devices with variable contact-resistance-area products R_cA of the MgO/Co electrodes. We explore the relationship between spin lifetime τ_s and charge-carrier mobility μ in SLG and find a similar $1/\mu$ dependence as seen in previous spin-transport studies on exfoliated BLG devices.[12] This dependence is only seen in samples with $R_cA > 1$ kΩ μm^2. In fact, we observe that devices with long τ_s additionally exhibit a second Dirac peak in charge transport, which stems from the electrodes. This contact-induced Dirac peak overlaps with the Dirac peak of the bare graphene, which complicates the analysis of the carrier mobility and thus complicates a clear assignment of the dominant spin scattering mechanism in graphene. For devices with small R_cA we find an overall strong decrease of τ_s, showing that transparent contacts yield additional spin dephasing in graphene underneath the contacts.

We have fabricated exfoliated SLG and BLG devices on SiO_2(300 nm)/Si^{++} wafers. The number of graphene layers is determined by optical contrast measurement, which is calibrated by Raman spectroscopy. After e-beam lithography we use molecular beam epitaxy to first grow an MgO spin injection/detection barrier with varying thicknesses up to 3 nm followed by 35-nm-thick ferromagnetic Co contacts. The rather thick barrier is necessary due to the fact that MgO on graphene grows in the Volmer-Weber mode (island formation) if no wetting layer is used.[23] We have evidence that even devices with large R_cA contacts that show nonlinear differential I-V curves still exhibit pinholes in the barrier.[24] Thus the exact current distribution through the contact areas is unknown, which complicates the assignment of the correct R_cA values.[25] For the sake of simplicity, we assume a homogeneous current distribution for our analysis.

All transport measurements are performed under vacuum condition at room temperature (RT) using standard lock-in techniques.[26] The highly doped Si^{++} wafer is used as a back gate, which allows changing the charge-carrier density $n = \alpha(V_G - V_D)$ in the graphene sheet according to the established capacitor model[27] with $\alpha \approx 7.18 \times 10^{10}$ V^{-1}cm^{-2}, with V_G being the applied gate voltage and V_D being the gate-voltage position of the maximum resistivity at the charge neutrality point, also called the Dirac point. By a linear fit of the conductance σ, we extract the charge-carrier mobility $\mu = (1/e)(\partial\sigma/\partial n)$ at an electron density of $n = 1.5 \times 10^{12}$ cm^{-2}. Hanle spin precession measurements are performed in standard nonlocal four-terminal geometry and are fitted by a simplified analytical solution[28,29] of the steady-state Bloch-Torrey equation:[26]

$$\frac{\partial \vec{s}}{\partial t} = \vec{s} \times \vec{\omega}_0 + D_s \nabla^2 \vec{s} - \frac{\vec{s}}{\tau_s} = 0, \qquad (1)$$

where $\vec{s}$ is the net spin vector, $\omega_0 = g\mu_B B/\hbar$ is the Larmor frequency, D_s is the spin-diffusion constant, and τ_s is the transverse spin lifetime. Recent experiments indicate that the effective g factor in graphene-based spin-transport devices may differ from the free-electron value at low temperatures after a hydrogen treatment.[30] As ESR measurements for

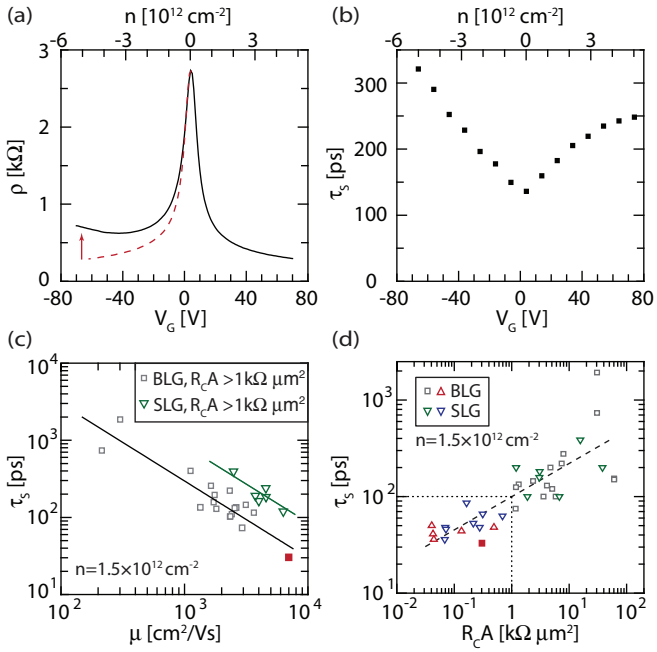

FIG. 1. (Color online) (a) ρ vs V_G of a SLG device with large R_cA. The increase towards negative V_G (see red arrow) indicates the existence of a second charge neutrality point. As a guide to the eye the electron branch for $V_G > 0$ is mirrored at the Dirac point (red dashed line). (b) τ_s vs V_G and n; the minimum at the Dirac point is typical for devices with large R_cA. (c) τ_s vs μ at $n = 1.5 \times 10^{12}$ cm^{-2} taken at RT for BLG (taken from Ref. 12) and SLG devices with large R_cA contacts. The lines are the best fit to a DP-like spin dephasing. The BLG device with the shortest spin lifetime (solid square) will be discussed separately in the text. (d) τ_s vs R_cA of all spin-transport devices in (c) and Fig. 2(a).

untreated graphene show $g \approx 2$ even for low temperatures[21,22] and we also restrict ourselves to RT, we assume $g = 2$ for all devices in this study.

In Figs. 1(a)–1(c) we show typical transport data for a SLG device with $R_cA > 1$ kΩ μm^2.[2,26] We first note that there is a strong electron-hole asymmetry in charge transport [Fig. 1(a)] as seen by the increase of the graphene resistivity for hole doping towards large negative V_G values. Its origin will be discussed further below. Spin lifetimes are extracted from Hanle curves,[12] which have been measured in perpendicular magnetic fields. The gate-voltage-dependent τ_s times in Fig. 1(b) show a minimum at the Dirac point and increase with both electron and hole doping. This general trend is observed for most large R_cA devices.

We next evaluate the dependence of τ_s on the electron mobility μ at $n = 1.5 \times 10^{12}$ cm^{-2} for all SLG devices in Fig. 1(c) (green triangles) on a log-log scale. For easier comparison we include results on BLG [gray squares in Fig. 1(c)], which some of us had previously measured.[12] The most striking observation is that, like in BLG, τ_s depends inversely on μ in our SLG devices. This relationship was previously attributed to the dominance of D'yakonov-Perel' (DP) spin dephasing in graphene.

Remarkably, SLG devices exhibit longer spin lifetimes than BLG devices of equal mobility. The vertical offset between SLG and BLG in Fig. 1(c) can be analyzed within the DP spin-dephasing mechanism. For this we replace the momentum scattering time τ_m in the DP formula $1/\tau_s = \Omega_{\text{eff}}^2(\Delta_{\text{SO}})\,\tau_m$ with the Boltzmann expression of the mobility $\mu = e\tau_m/m_{\text{eff}}^*$ and take the logarithm:[28]

$$\ln(\tau_s) = \ln\left(\frac{e}{\Omega_{\text{eff}}^2(\Delta_{\text{SO}})\,m_{\text{eff}}^*}\right) - \ln(\mu), \qquad (2)$$

where e is the elementary charge, Ω_{eff}^2 is the effective Larmor frequency, which is dependent on the spin-orbit coupling Δ_{SO}, and m_{eff}^* is the effective mass. With this expression it is obvious that the vertical offset in Fig. 1(c) can either result from a smaller effective mass or a smaller overall spin-orbit coupling strength in the SLG devices. We note that SLG is expected to exhibit massless Dirac fermions near the Dirac point only in simple tight-binding approximations. It has been shown that even the small intrinsic spin-orbit coupling in SLG gives rise to a small effective mass of the charge carriers,[31,32] which supports our simple approach in Eq. (2). Even stronger effects are expected from extrinsic sources such as contacts, adatoms, and the underlying substrate.[14,16,17] As all experimental values of τ_s are well below theoretical predictions, we expect that spin relaxation and dephasing is governed by extrinsic sources in present devices. Because of the dominant extrinsic contribution to the spin-orbit coupling slight changes in the fabrication steps between the BLG and SLG devices (in our case another batch of wafers and a different resist for the lithography process) might be the reason for the observed offset in the lifetime. These changes in sample fabrication may also explain the overall larger carrier mobilities in the new series of SLG devices seen in Fig. 1(c) (no device under 2000 cm^2/Vs).

In the following, we will focus on the influence of R_cA on τ_s. Several groups have suggested using highly resistive tunneling contacts to avoid the backflow of charge-carrier spins into the ferromagnetic electrodes which otherwise yields a reduction of the spin lifetime.[2,19,20,33] As mentioned above, all of our SLG devices exhibit large R_cA values. Revisiting our previous BLG measurements also reveals R_cA values above 1 kΩ μm^2 for almost all BLG data points in Fig. 1(c) (gray squares). Only the BLG device with the highest mobility [solid red square in Fig. 1(c)] has small R_cA contacts with a flat differential dI/dV curve.[26]

At first sight this red data point seems to follow the DP-like trend of the large R_cA BLG devices. To explore this in further detail we fabricated additional SLG and BLG samples with a thinner MgO barrier but otherwise the same fabrication procedure. All of those samples show $R_cA <$ 1 kΩ μm^2 [Fig. 1(d), blue and red data points]. As seen in Fig. 2(a), they exhibit strongly reduced τ_s values which vary between 30 and 70 ps (upward-pointing triangles for BLG and downward-pointing ones for SLG) and lie well below all large R_cA devices with no significant difference between SLG and BLG devices. Furthermore, the data do not follow the $1/\mu$ dependence. It is therefore obvious that devices with $R_cA < 1$ kΩ μm^2 exhibit short spin lifetimes in which the above μ dependence of the large R_cA devices is hidden by an additional spin-dephasing channel which most likely results from the contacts.

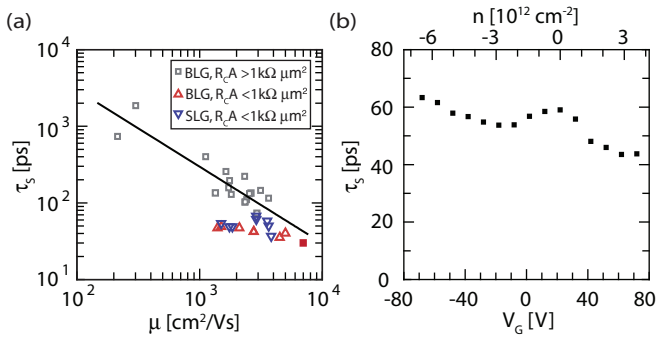

FIG. 2. (Color online) (a) τ_s vs μ taken at $n = 1.5 \times 10^{12}$ cm^{-2} at 300 K. Squares are taken from Ref. 12; upward- and downward-pointing triangles are BLG and SLG devices, respectively. Both exhibit $R_cA < 1$ kΩ µm^2. (b) τ_s vs V_G dependence of a typical device with transparent contacts.

The strong influence of small R_cA contacts on the spin transport can also be seen by the charge-density dependence of τ_s [Fig. 2(b)], which is similar for all small R_cA devices. In contrast to all large R_cA devices at room temperature [see Fig. 1(b)], τ_s does not increase away from the Dirac point, but it rather decreases and may increase again at larger carrier densities. Although we presently do not understand this qualitative change in the density dependence, we note that such a decrease of τ_s has previously also been observed in BLG devices with large R_cA contacts at low temperatures.[12]

While we have seen that devices with small and large R_cA values show a distinctly different mobility dependence of the spin lifetime [Figs. 1(c) and 2(a)], we now discuss the dependence of τ_s on R_cA, which is shown in Fig. 1(d) for all devices with measured R_cA values. We note that even within a single device the respective R_cA values for different contacts may vary significantly. The plotted R_cA values in Fig. 1(d) are thus mean values of the respective injector and detector contacts of each device. Remarkably, we observe a significant increase of τ_s with R_cA for all devices, suggesting that the contacts are even the bottleneck for the large R_cA devices. However, these devices also showed the pronounced inverse dependence of τ_s on μ [see Fig. 1(c)]. It is therefore interesting to study if the influence of the contacts also becomes evident in charge transport.

In Figs. 3(a) to 3(c), we summarize the gate-voltage-dependent graphene resistivity for both large and small R_cA SLG and BLG devices. While we only observe one Dirac peak around zero gate voltage in all small R_cA devices [see Fig. 3(c)], we typically observe a second Dirac peak at larger negative gate voltages for SLG and BLG devices with large R_cA [Figs. 3(a) and 3(b)]. Such a second Dirac peak has already been observed in spin-valve devices by another group.[34] The resistivity ratio of both Dirac peaks varies significantly from device to device. Not all large R_cA devices show the maximum of the second Dirac peak for $V_G > -80$ V [compare to Fig. 1(a)]. But the general trend is that the separation between both Dirac peaks gets smaller for devices with larger R_cA. Consistent with the additional scaling between R_cA and τ_s, the smallest peak separation has been observed in the device with the longest τ_s of 2 ns [Fig. 3(b)].

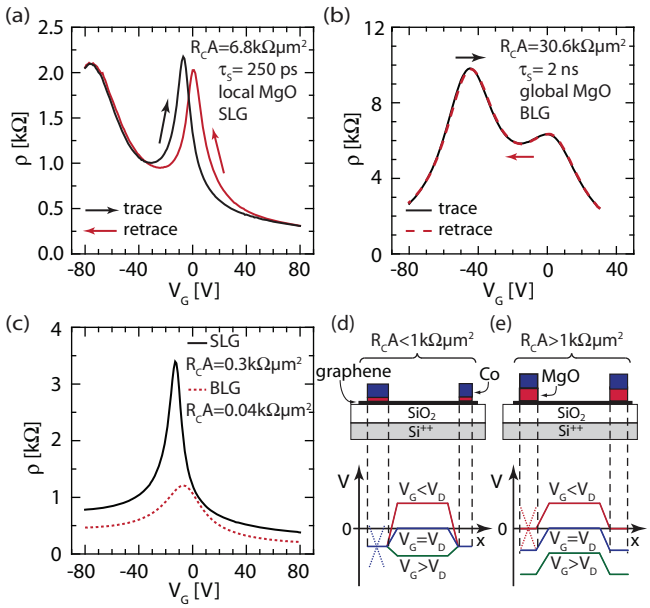

FIG. 3. (Color online) (a) ρ vs V_G of a large R_cA SLG device with $\tau_s = 250$ ps showing a pronounced contact-induced second Dirac peak at $V_G = -75$ V. This Dirac peak does not show any hysteresis in contrast to the Dirac peak of the bare graphene near $V_G = 0$ V. The arrows indicate the sweep directions of the gate voltage. (b) ρ vs V_G for a large R_cA BLG device with $\tau_s = 2$ ns [see Fig. 2(a)] and completely MgO covered graphene. No hysteresis is visible. (c) ρ vs V_G of SLG and BLG devices with small R_cA contacts. In addition to a doping, the contacts may screen the gate field V_G, which can result in (d) pinning (small R_cA) or (e) no pinning (large R_cA) of the electrostatic potential under the contacts (corresponding Dirac cones indicated).

The left Dirac peak most likely results from the magnetic electrodes, while the right Dirac peak is due to charge transport through the graphene sheet between the electrodes. This notion is supported by hysteresis measurements when comparing different devices with local and global MgO barriers. In the former case MgO is only deposited underneath the ferromagnetic electrodes [see Fig. 3(a) for the corresponding SLG device], while in the latter case MgO completely covers the graphene flake [see Fig. 3(b)]. A hysteresis is only observed for the right Dirac peak in the device with local MgO barriers [Fig. 3(a)]. It can originate from a thin water film on top of the graphene flake.[35] Although we measure under vacuum conditions, such a hysteresis is initially always observed before the water eventually evaporates after a few hours. However, no hysteresis for the left Dirac peak at negative gate voltages is observed. If this peak results from the contact area, this is also expected as water cannot cover the graphene underneath the contact area. Consistent with this assessment, we do not observe any hysteresis for global MgO devices [see Fig. 3(b)].

We next link the appearance of the second Dirac peak to the measured spin lifetime and the contact characteristics. It is well known that the contact material has a great influence on the transport properties in graphene. Scanning photocurrent microscopy experiments, for example, directly probe contact-induced doping and show Fermi-level pinning from metallic electrodes.[36] A gate-voltage-dependent doping profile of the electrostatic potential V for devices with low Ohmic contacts

is depicted in Fig. 3(d). Here $-eV$ equals the position of the Fermi level in the graphene band structure. Although this profile can successfully explain an electron-hole asymmetry in the resistivity,[37] which we also observe in our small R_cA devices, it cannot explain the second Dirac peak as the carrier density underneath the electrodes is not affected by the gate voltage.

As noted above, there is an island growth of our MgO barriers. In particular for thin barriers this favors the formation of conducting Co pinholes with presumably direct contact of the Co to the graphene layer. As shown by recent angle-resolved photoemission spectroscopy, the Dirac cone of graphene is strongly shifted into the valence band for Co/graphene interfaces, and its π^* band hybridizes with $3d$ bands of Co near the Fermi level.[38,39] This hybridization is consistent with the Fermi-level pinning in our small R_cA devices. It furthermore might account for the reduced spin lifetimes in Fig. 2(a) (red and blue data points) as the injected spins might be scattered by the $3d$ states in the graphene layer.

For large R_cA devices with thicker MgO oxide barriers the formation of pinholes is suppressed. Accordingly, the $3d$ hybridization of Co with graphene states gets diminished, which can yield longer spin lifetimes. Furthermore, we expect a gradual depinning of the Fermi level. Together with the weaker Co-induced n doping with increasing oxide thickness[40,41] this also explains the appearance of the second Dirac peak. This situation is illustrated in Fig. 3(e), where the back-gate voltage now also tunes the carrier density underneath the contacts. We note that the transition between pinning and depinning should, in principal, be continuous with increasing R_cA. In other words, the appearance of the second Dirac peak does not necessarily imply a complete depinning. Considering the spatially inhomogeneous barrier thickness due to the Volmer-Weber island growth and remaining pinholes even for large R_cA devices, all current devices might not be in the regime of complete depinning. The rough Co/MgO interface may also result in inhomogeneous local magnetic fields, which can be an additional source of spin dephasing.[42] Finally, we do not observe a systematic dependence of the amplitude of the spin signal on the R_cA values,[26] which excludes a backflow of spins into the ferromagnetic electrode as a possible explanation of the observed τ_s dependence on R_cA.[19,20,33]

Next we address the calculation of μ for devices with a second Dirac peak. In Figs. 1(c) and 2(a) we determined μ and n from the right Dirac peak, which we attribute to the bare-graphene part. This might be a good approach for devices with only one Dirac peak [Fig. 3(c)] or for devices where the left Dirac peak is strongly separated in gate voltage as in Fig. 1(a). In particular for devices with long τ_s, however, the two Dirac peaks are not well separated but strongly overlap, as seen in Figs. 3(a) and 3(b) for large R_cA SLG and BLG devices, respectively. This overlapping has a significant influence on the slope $\partial\rho/\partial V_G$ of the right Dirac peak at $n = 1.5 \times 10^{12}$ cm^{-2} ($V_G - V_D \approx 20$ V). The smaller the separation between both Dirac peaks becomes, the smaller the respective slope and carrier mobility will be. We note that this results in an underestimation of the mobility of the bare-graphene part. It is important to emphasize that the contact-induced left Dirac peak might thus partially be responsible for the decrease in observed carrier mobility for devices with longer spin lifetimes.

There are more elaborate models to determine carrier mobilities, including contact-induced pinning and depinning of the Fermi level and the respective potential profiles of the graphene along the device.[34,43–46] However, there are too many unknown quantities which currently hinder extracting reliable values for the respective carrier mobilities in the different graphene parts from a single gate-dependent resistivity measurement.[26] Without further measurements of the potential profile we thus cannot give a more precise evaluation of the influence of the contact-induced Dirac peak on the carrier mobility. This, on the other hand, would be important for identifying intrinsic spin-dephasing mechanisms in graphene. Our findings show that understanding spin transport in graphene-based nonlocal spin-valve devices requires independent understanding of both spin- and charge-transport properties, which may significantly differ in graphene underneath the spin injection and detection electrodes and graphene between the electrodes.[5]

In summary, we have studied spin and charge transport in graphene-based nonlocal spin-valves by tuning the R_cA values of MgO injection/detection barriers. For small R_cA contacts, there is a significant spin dephasing in graphene underneath the contacts, while SLG and BLG devices with large R_cA values show long spin lifetimes at RT. The latter devices exhibit a second Dirac peak at negative gate voltages. As the peak separation is smallest for devices with the longest spin lifetimes, it might partially account for the observed $1/\mu$ dependence of τ_s.

This work was supported by DFG through FOR 912.

*bernd.beschoten@physik.rwth-aachen.de

[1] N. Tombros, C. Jozsa, M. Popinciuc, H. T. Jonkman, and B. J. van Wees, Nature (London) **448**, 571 (2007).

[2] B. Dlubak, M.-B. Martin, C. Deranlot, B. Servet, S. Xavier, R. Mattana, M. Sprinkle, C. Berger, W. A. De Heer, F. Petroff, A. Anane, P. Seneor, and A. Fert, Nat. Phys. **8**, 557 (2012).

[3] W. Han and R. K. Kawakami, Phys. Rev. Lett. **107**, 047207 (2011).

[4] W. Han, J.-R. Chen, D. Wang, K. M. McCreary, H. Wen, A. G. Swartz, J. Shi, and R. K. Kawakami, Nano Lett. **12**, 3443 (2012).

[5] M. H. D. Guimaraes, A. Veligura, P. J. Zomer, T. Maassen, I. J. Vera-Marun, N. Tombros, and B. J. van Wees, Nano Lett. **12**, 3512 (2012).

[6] A. G. Swartz, J.-R. Chen, K. M. McCreary, P. M. Odenthal, W. Han, and R. K. Kawakami, Phys. Rev. B **87**, 075455 (2013).

[7] B. Birkner, D. Pachniowski, A. Sandner, M. Ostler, T. Seyller, J. Fabian, M. Ciorga, D. Weiss, and J. Eroms, Phys. Rev. B **87**, 081405 (2013).

[8] S. Jo, D.-K. Ki, D. Jeong, H.-J. Lee, and S. Kettemann, Phys. Rev. B **84**, 075453 (2011).

[9] I. Neumann, J. Van de Vondel, G. Bridoux, M. V. Costache, F. Alzina, C. M. S. Torres, and S. O. Valenzuela, Small **9**, 156 (2013).

[10] M. Wojtaszek, I. J. Vera-Marun, T. Maassen, and B. J. van Wees, Phys. Rev. B **87**, 081402 (2013).

[11]T. Maassen, J. J. van den Berg, N. IJbema, F. Fromm, T. Seyller, R. Yakimova, and B. J. van Wees, Nano Lett. **12**, 1498 (2012).
[12]T.-Y. Yang, J. Balakrishnan, F. Volmer, A. Avsar, M. Jaiswal, J. Samm, S. R. Ali, A. Pachoud, M. Zeng, M. Popinciuc, G. Güntherodt, B. Beschoten, and B. Özyilmaz, Phys. Rev. Lett. **107**, 047206 (2011).
[13]D. Huertas-Hernando, F. Guinea, and A. Brataas, Phys. Rev. Lett. **103**, 146801 (2009).
[14]C. Ertler, S. Konschuh, M. Gmitra, and J. Fabian, Phys. Rev. B **80**, 041405 (2009).
[15]K. Pi, W. Han, K. M. McCreary, A. G. Swartz, Y. Li, and R. K. Kawakami, Phys. Rev. Lett. **104**, 187201 (2010).
[16]A. H. Castro Neto and F. Guinea, Phys. Rev. Lett. **103**, 026804 (2009).
[17]P. Zhang and M. W. Wu, New J. Phys. **14**, 033015 (2012).
[18]A. Avsar, T.-Y. Yang, S. Bae, J. Balakrishnan, F. Volmer, M. Jaiswal, Z. Yi, S. R. Ali, G. Güntherodt, B. H. Hong, B. Beschoten, and B. Özyilmaz, Nano Lett. **11**, 2363 (2011).
[19]W. Han, K. Pi, K. M. McCreary, Y. Li, J. J. I. Wong, A. G. Swartz, and R. K. Kawakami, Phys. Rev. Lett. **105**, 167202 (2010).
[20]T. Maassen, I. J. Vera-Marun, M. H. D. Guimarães, and B. J. van Wees, Phys. Rev. B **86**, 235408 (2012).
[21]S. S. Rao, A. Stesmans, J. van Tol, D. V. Kosynkin, A. Higginbotham-Duque, W. Lu, A. Sinitskii, and J. M. Tour, ACS Nano **6**, 7615 (2012).
[22]M. A. Augustyniak-Jablokow, K. Tadyszak, M. Mackowiak, and S. Lijewski, Chem. Phys. Lett. **557**, 118 (2013).
[23]W. H. Wang, W. Han, K. Pi, K. M. McCreary, F. Miao, W. Bao, C. N. Lau, and R. K. Kawakami, Appl. Phys. Lett. **93**, 183107 (2008).
[24]F. Volmer, M. Drögeler, E. Maynicke, N. von den Driesch, M. L. Boschen, G. Güntherodt, and B. Beschoten (unpublished).
[25]K. Nagashio, T. Nishimura, K. Kita, and A. Toriumi, Appl. Phys. Lett. **97**, 143514 (2010).
[26]See Supplemental Material at http://link.aps.org/supplemental/10.1103/PhysRevB.88.161405 for a more detailed description of device fabrication, measurement methods, and supporting measurements.
[27]K. S. Novoselov, A. K. Geim, S. V. Morozov, D. Jiang, Y. Zhang, S. V. Dubonos, I. V. Grigorieva, and A. A. Firsov, Science **306**, 666 (2004).
[28]J. Fabian, A. Matos-Abiague, C. Ertler, P. Stano, and I. Žutić, Acta Phys. Slovaca **57**, 565 (2007).
[29]M. Johnson and R. H. Silsbee, Phys. Rev. B **37**, 5312 (1988).
[30]K. M. McCreary, A. G. Swartz, W. Han, J. Fabian, and R. K. Kawakami, Phys. Rev. Lett. **109**, 186604 (2012).
[31]M. Gmitra, S. Konschuh, C. Ertler, C. Ambrosch-Draxl, and J. Fabian, Phys. Rev. B **80**, 235431 (2009).
[32]S. Konschuh, M. Gmitra, and J. Fabian, Phys. Rev. B **82**, 245412 (2010).
[33]M. Popinciuc, C. Józsa, P. J. Zomer, N. Tombros, A. Veligura, H. T. Jonkman, and B. J. van Wees, Phys. Rev. B **80**, 214427 (2009).
[34]I. J. Vera-Marun, V. Ranjan, and B. J. van Wees, Nat. Phys. **8**, 313 (2012).
[35]H. Wang, Y. Wu, C. Cong, J. Shang, and T. Yu, ACS Nano **4**, 7221 (2010).
[36]T. Mueller, F. Xia, M. Freitag, J. Tsang, and P. Avouris, Phys. Rev. B **79**, 245430 (2009).
[37]R. Nouchi and K. Tanigaki, Appl. Phys. Lett. **96**, 253503 (2010).
[38]A. Varykhalov and O. Rader, Phys. Rev. B **80**, 035437 (2009).
[39]A. Varykhalov, D. Marchenko, J. Sanchez-Barriga, M. R. Scholz, B. Verberck, B. Trauzettel, T. O. Wehling, C. Carbone, and O. Rader, Phys. Rev. X **2**, 041017 (2012).
[40]G. Giovannetti, P. A. Khomyakov, G. Brocks, V. M. Karpan, J. van den Brink, and P. J. Kelly, Phys. Rev. Lett. **101**, 026803 (2008).
[41]M. Bokdam, P. A. Khomyakov, G. Brocks, and P. J. Kelly, Phys. Rev. B **87**, 075414 (2013).
[42]S. P. Dash, S. Sharma, J. C. Le Breton, J. Peiro, H. Jaffrès, J.-M. George, A. Lemaître, and R. Jansen, Phys. Rev. B **84**, 054410 (2011).
[43]S. A. Thiele, J. A. Schaefer, and F. Schwierz, J. Appl. Phys. **107**, 094505 (2010).
[44]D. Jimenez, IEEE Trans. Electron Devices **58**, 4377 (2011).
[45]R. Nouchi and K. Tanigaki, Jpn. J. Appl. Phys. **50**, 070109 (2011).
[46]Q. Li, E. H. Hwang, E. Rossi, and S. Das Sarma, Phys. Rev. Lett. **107**, 156601 (2011).